Supplemental Material

Exotic magnetism in perovskite $KOsO_3$

Jie Chen[1], Hongze Li[1], Javier Gainza[2], Angel Munoz[3], Jose A. Alonso[2], Jue Liu[4], Yu-Sheng Chen[5], Alexei A. Belik,[6] Kazunari Yamaura,[6,7] Jiaming He[1], Xinyu Li[1], John B. Goodenough[1], and J.-S. Zhou[1*]

[1] Materials Science and Engineering program, Mechanical Engineering, University of Texas at Austin, Austin, TX 78712 USA

[2] Instituto de Ciencia de Materiales de Madrid, CSIC, Cantoblanco, E-28049 Madrid, Spain

[3] Universidad Carlos III, Avenida Universidad 30, E-28911, Leganés-Madrid, Spain

[4] Neutron Scattering Division, Oak Ridge National Laboratory, Oak Ridge, Tennessee 37830, USA

[5] NSF's ChemMatCARS, The University of Chicago, Illinois 60437, USA

[6] Research Center for Materials Nanoarchitectonics (MANA), National Institute for Materials Science, Namiki 1-1, Tsukuba, Ibaraki 305-0044, Japan

[7] Graduate School of Chemical Sciences and Engineering, Hokkaido University, North 10 West 8, Kita-ku, Sapporo, Hokkaido 060-0810, Japan

Material preparation

Polycrystalline and single-crystal perovskite $KOsO_3$ were synthesized by solid-state reaction under high-pressure and high-temperature conditions. The starting materials KO_2 (O_2-45.6 %, Sigma-Aldrich), OsO_2 (Os-84.0%, Alfa Aesar), and Os (99.95%, Alfa Aesar) in the molar ratio KO_2: OsO_2: Os = 1.15:0.7:0.3 were thoroughly mixed and ground in an Ar-filled glove box. It is necessary to add 15 mol% excessive KO_2 for reducing the impurity of Os in the final products. The mixture was pressed and sealed into a Pt capsule, which was also operated in the Ar-filled glove box. Then, the sealed Pt capsule filled with starting materials is inserted into a cylindrical $LaCrO_3$ sleeve; the Pt capsule acts as a heater. The $LaCrO_3$ sleeve, Pt capsule and two current rings are placed in a Cr-doped MgO octahedron with 12 mm edge length. The high-pressure and high-temperature synthesis was performed with a Walker-type multi-anvil module (Rockland Research Co.) by using 6/12 sample assembly (carbide anvils with 6-mm truncation and 12-mm octahedron). A pressure of 14 GPa was statically generated, followed by heating at a temperature of 1000-1200 °C for the polycrystalline sample and 1300 °C for the single-crystal sample and keeping the temperature for 30 min. The sample was quenched to room temperature within a minute by cutting off the power supply before the pressure was gradually released.

Determination of the crystal structure by synchrotron X-ray single crystal diffraction

Single-crystal X-ray diffraction measurements were carried out at NSF's ChemMatCARS, Sector 15 of APS at Argonne National Laboratory with the X-ray wavelength λ = 0.41328 Å. A crystal of size 10 × 10 × 10 μm^3 was mounted on the tip of a glass fiber. The experiments were performed at temperatures between 200 and 300 K. Data were collected by a Pilatus 1M (CdTe) detector. The cbf frames were converted to Bruker's sfrm format, and Bruker APEX 3 suite software was used for data integration. Data reduction was carried out with the SAINT V8. 40B and SADABS v.2016 programs included in the APEX suite. The full-matrix least-squares refined the single-crystal structure at each temperature on F^2 with the Olex2 1.5 program. The structure refinement data and bond length are shown in Table S1, S2 and S3 of Supplemental Material.

Determination of the crystal structure by X-ray powder diffraction

(1) Each batch of samples was initially checked by using X-ray powder diffraction (XRD) with the in-house diffractometer RIGAKU-MiniFlex 600 with Cu-Kα radiation at room temperature.

(2) Samples from selected batches were further measured by using synchrotron X-ray diffraction at 11-BM of Advanced Photon Source (APS) with the synchrotron X-ray wavelength λ = 0.459607 Å at room temperature and at SPring-8 with the wavelength λ = 0.61928 Å at temperatures from 100 to 500 K. These data were analyzed with Rietveld refinement by using the RIETAN-FP and VESTA software [10,11].

Determination of the magnetic structure by neutron diffraction

The Time-of-Flight (TOF) Neutron diffraction patterns at temperatures of 100 K, 200 K, 300 K, 400 K, and 500 K were collected by the Nanoscale Ordered Materials Diffractometer (NOMAD) of Spallation Neutron located at Oak Ridge National Laboratory. NOMAD is a high flux, medium resolution neutron diffractometer, allowing the neutron diffraction measurements on very small samples (e.g., tens to hundreds of mg)[12,13]. The polycrystalline $KOsO_3$ sample of 300 mg was loaded into a 3 mm quartz capillary and sealed for the measurements. The sample temperature was controlled using Ar cryostream; sample was equilibrated at each temperature points for 10 min before taking the specific temperature scans. Two 24 min scans (2C each) were collected and summed together to improve the statistics. The collected neutron diffraction data were background subtracted (empty quartz capillary) and normalized to against the scattering from a 6 mm V rod. The refinements of the different patterns were performed by the Rietveld method with the Fullprof software [14] against data collected with the detector banks 1 and 2 at 2θ of 31° and 67°. The Neutron diffraction patterns at temperatures (= 100, 200, 300, 400, and 500 K) and fitting results are shown in Fig. S10 of Supplemental Material. In addition, the possible magnetic structures compatible with the $KOsO_3$ symmetry were determined by considering the theory of group representations described by Bertaut [15] and using the GBASIREPS program of the Fullprof package. Irreducible representations for the little group are tabulated in Table S7 of Supplemental Material.

Measurements of physical properties

The electron transport measurement was performed on a single crystal of $KOsO_3$ between 2 and 300 K by the four-probe method in the van der Pauw configuration with a physical property measurement system (PPMS, Quantum Design, Inc.).

The magnetic properties were measured in a magnetic property measurement system (MPMS, Quantum Design, Inc.). The polycrystalline sample wrapped with a copper foil was used for the measurement. The contribution of the copper capsule was subtracted from the raw data.

The measurement of heat capacity (C_p) was conducted in PPMS. A dense pellet used for the C_p measurement was pressed from the polycrystalline $KOsO_3$ (13.09 mg), and Apiezon-N grease was used to mount the sample in the puck for the C_p measurement. The thermoelectric power (S) of the powder sample was collected by the thermal transport option of PPMS and the two-probe lead configuration method was employed. The powder sample was loaded into a 0.7 mm diameter hole on a hard-plastic die and small pieces of Indium metal were used to cover both ends. Identical results of the thermoelectric power were obtained in a single crystal sample of other material and the powder made by pulverizing the crystal which was loaded in the die.

Differential scanning calorimetry (DSC) measurement was conducted on polycrystalline $KOsO_3$ (9.06 mg) using a Mettler Toledo DSC1 STAR^e system at a heating-cooling rate of 20 or 30 K/min between 173 K and 403 K. The sample, sealed in an aluminum capsule, underwent multiple runs of DSC measurements to confirm its reproducibility.

Density functional theory calculation

First-principles calculations were performed using spin-polarized density functional theory with Vienna Ab initio simulation package (VASP). Both PBEsolid+U and PBEsolid+U+SOC functional and projector augmented wave (PAW) potentials were employed in our simulations.[16-19] U = 1.7 eV and J_H = 0.7 eV were employed for the description of Os-ion orbitals. Spin-orbital coupling effect was included in the simulation. We selected PAW potentials for K, Os and O with the electronic configurations $3s^2 3p^6 4s^1$, $5d^6 5p^6 6s^2$, $2s^2 2p^4$. A supercell of 40 atoms was employed in our simulations. All calculations were performed on 5 × 5 × 5 Monkhorst-Pack mesh and 600 eV plane wave cutoff. Band structures and fermi surface were visualized using PyProcar[20] and XCrySDen[21] codes, respectively.

It becomes not practical to simulate the electronic structure on the base of a larger cell that covers the incommensurate modulation of magnetic moment. The G-type AFM has been found to be the ground state in the primary cubic perovskite cell. The comparison of the cell energy in different types of magnetic ordering can be found in Table S9, S10. A metallic phase can be obtained with the calculation DFT + U=1 eV + SOC and the density of states at the Fermi energy is $N(E_F)$=1.8 States/(eV f.u.).

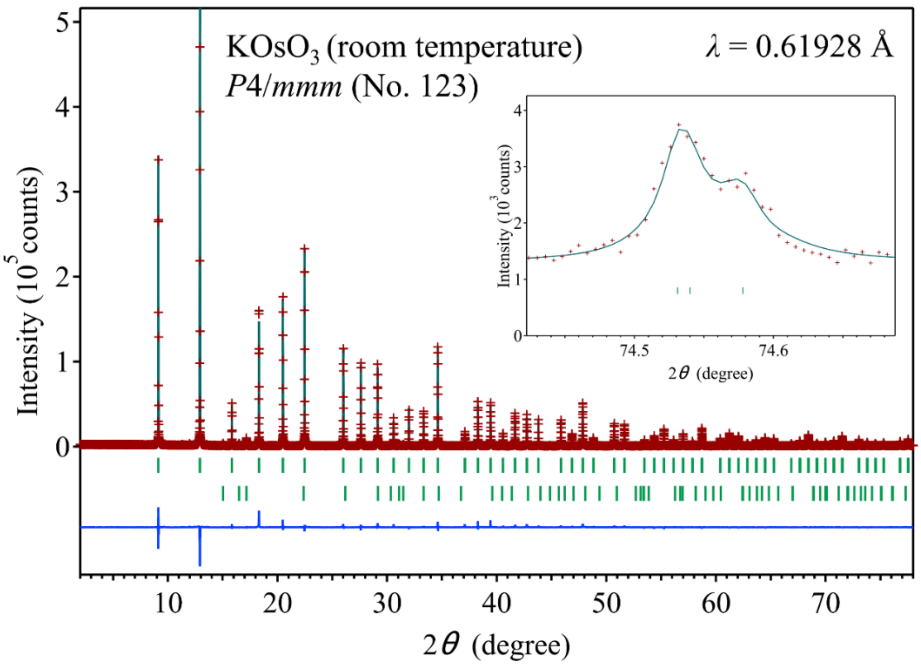

Fig. S1 The pattern of powder XRD (λ = 0.61928 Å) collected at room temperature and the result of Rietveld refinement based on tetragonal structural model *P4/mmm* (No. 123). The crosses and solid lines show the observed and calculated patterns, respectively, with their differences shown at the bottom. The expected Bragg reflections for the perovskite phase of $KOsO_3$ (97.44 wt%) are marked by upper ticks and Os impurity (2.56 wt%) are marked by lower ticks.

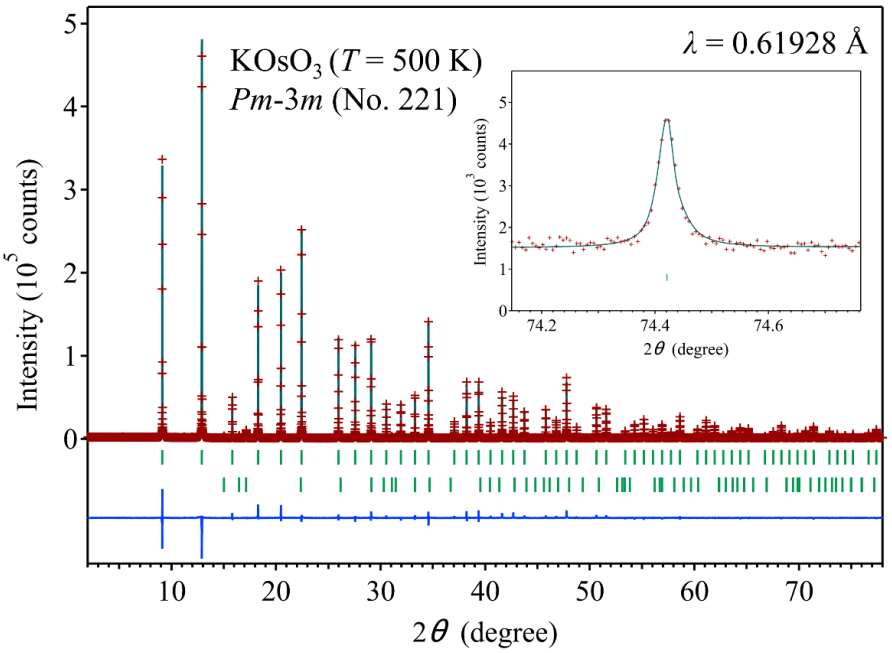

Fig. S2 The pattern of powder XRD (λ = 0.61928 Å) collected at 500 K and the result of Rietveld refinement based on cubic structural model *Pm*-3*m* (No. 221). The crosses and solid lines show the observed and calculated patterns, respectively, with their differences shown at the bottom. The expected Bragg reflections for the perovskite phase of $KOsO_3$ (97.38 wt%) are marked by upper ticks and Os impurity (2.62 wt%) are marked by lower ticks.

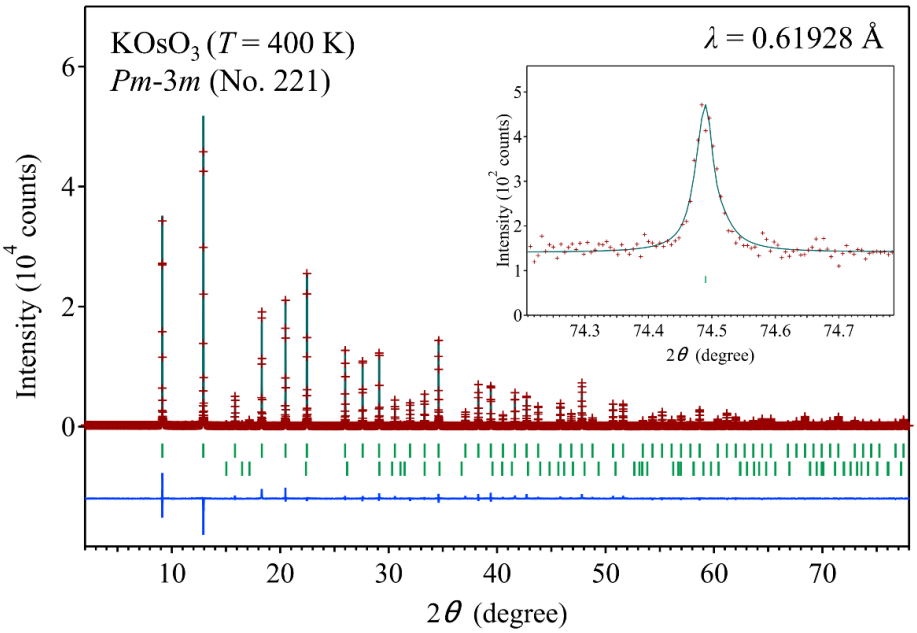

Fig. S3 The pattern of powder XRD (λ = 0.61928 Å) collected at 400 K and the result of Rietveld refinement based on cubic structural model *Pm*-3*m* (No. 221). The crosses and solid

lines show the observed and calculated patterns, respectively, with their differences shown at the bottom. The expected Bragg reflections for the perovskite phase of $KOsO_3$ (97.31 wt%) are marked by upper ticks and Os impurity (2.69 wt%) are marked by lower ticks.

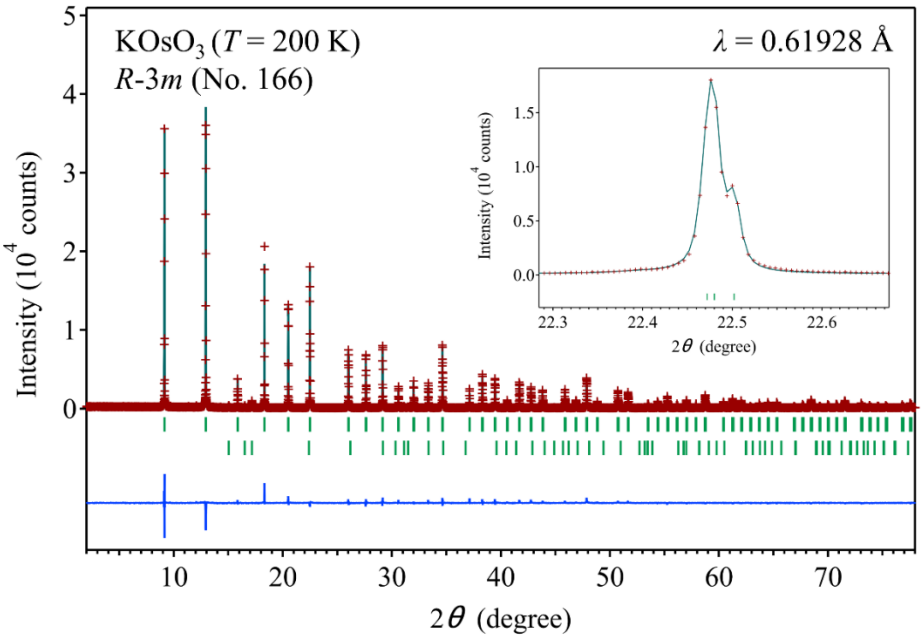

Fig. S4 The pattern of powder XRD (λ = 0.61928 Å) collected at 200 K and the result of Rietveld refinement based on rhombohedral structural model *R*-3*m* (No. 166). The crosses and solid lines show the observed and calculated patterns, respectively, with their differences shown at the bottom. The expected Bragg reflections for the perovskite phase of $KOsO_3$ (97.48 wt%) are marked by upper ticks and Os impurity (2.52 wt%) are marked by lower ticks.

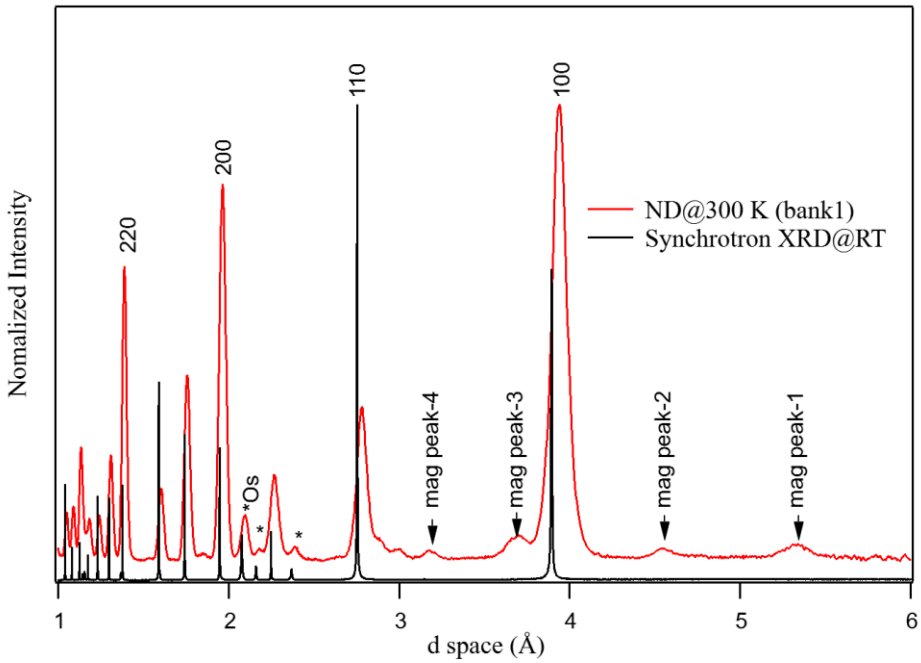

Fig.S5 X-ray powder diffraction and neutron diffraction from bank1.

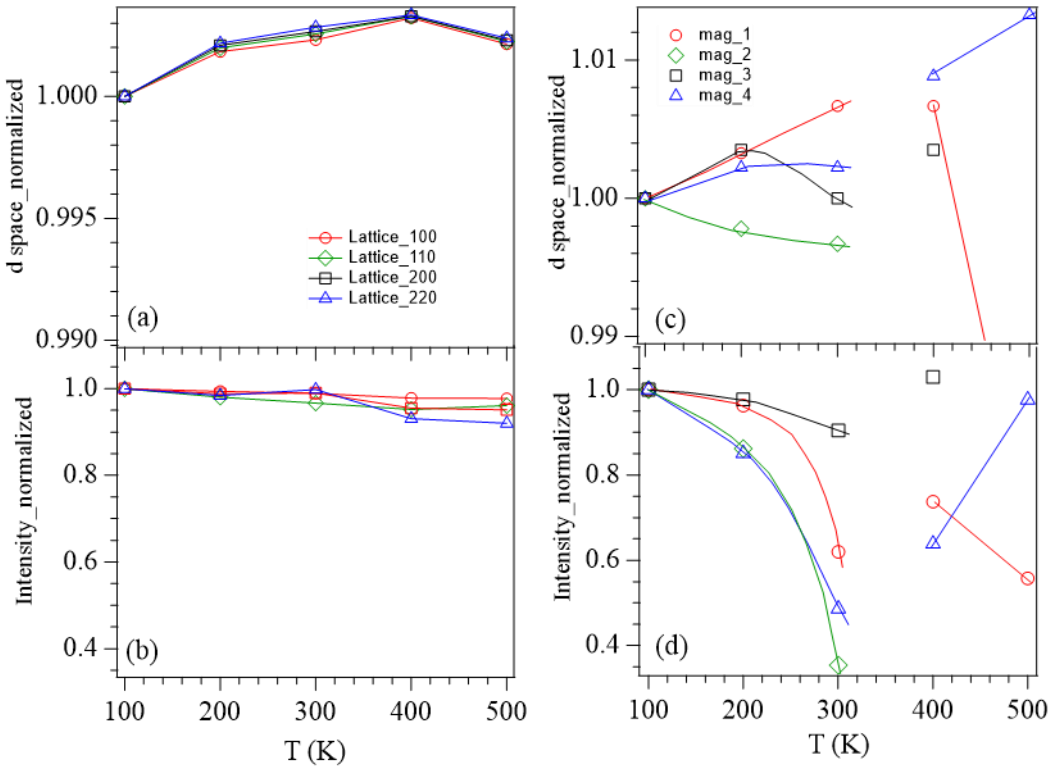

Fig.S6 Temperature dependences of peak intensity and d value of lattice diffraction and the possible magnetic diffraction peaks.

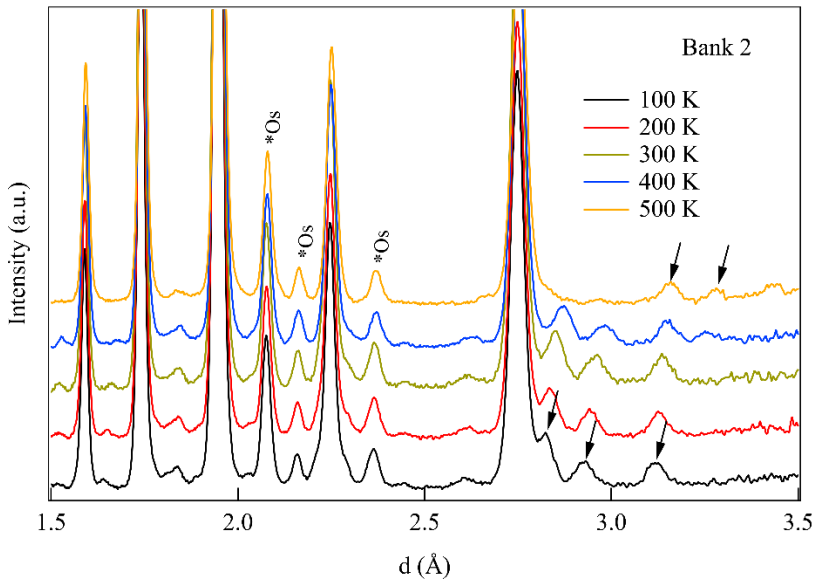

Fig. S7 Neutron powder diffraction (bank 2) at different temperatures

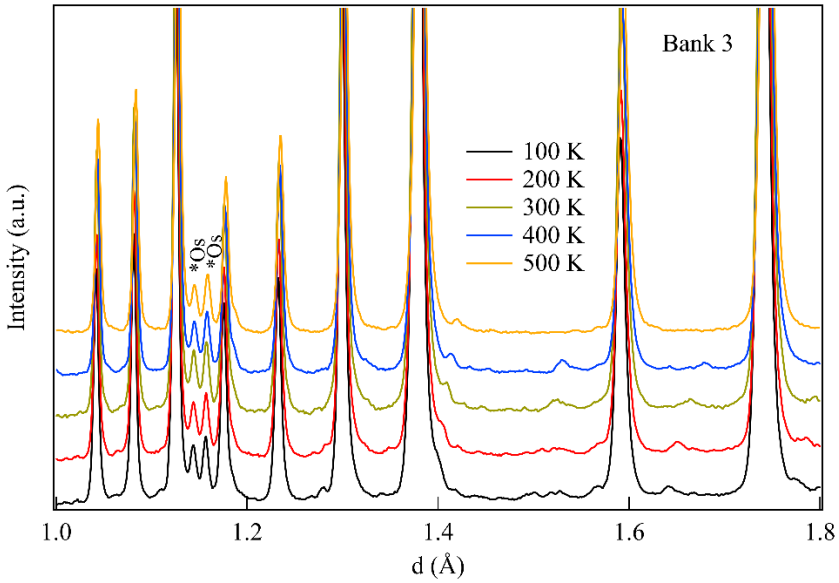

Fig. S8 Neutron powder diffraction (bank 3) at different temperatures

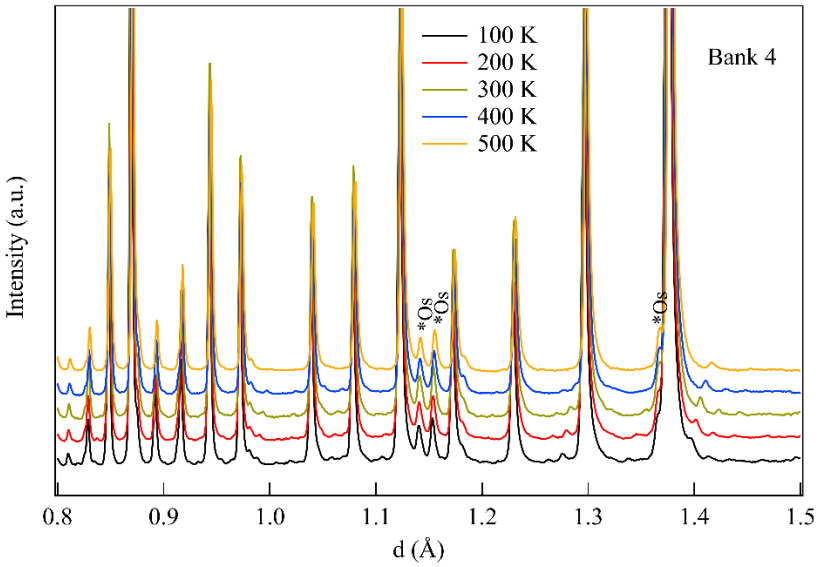

Fig. S9 Neutron powder diffraction (bank 4) at different temperatures

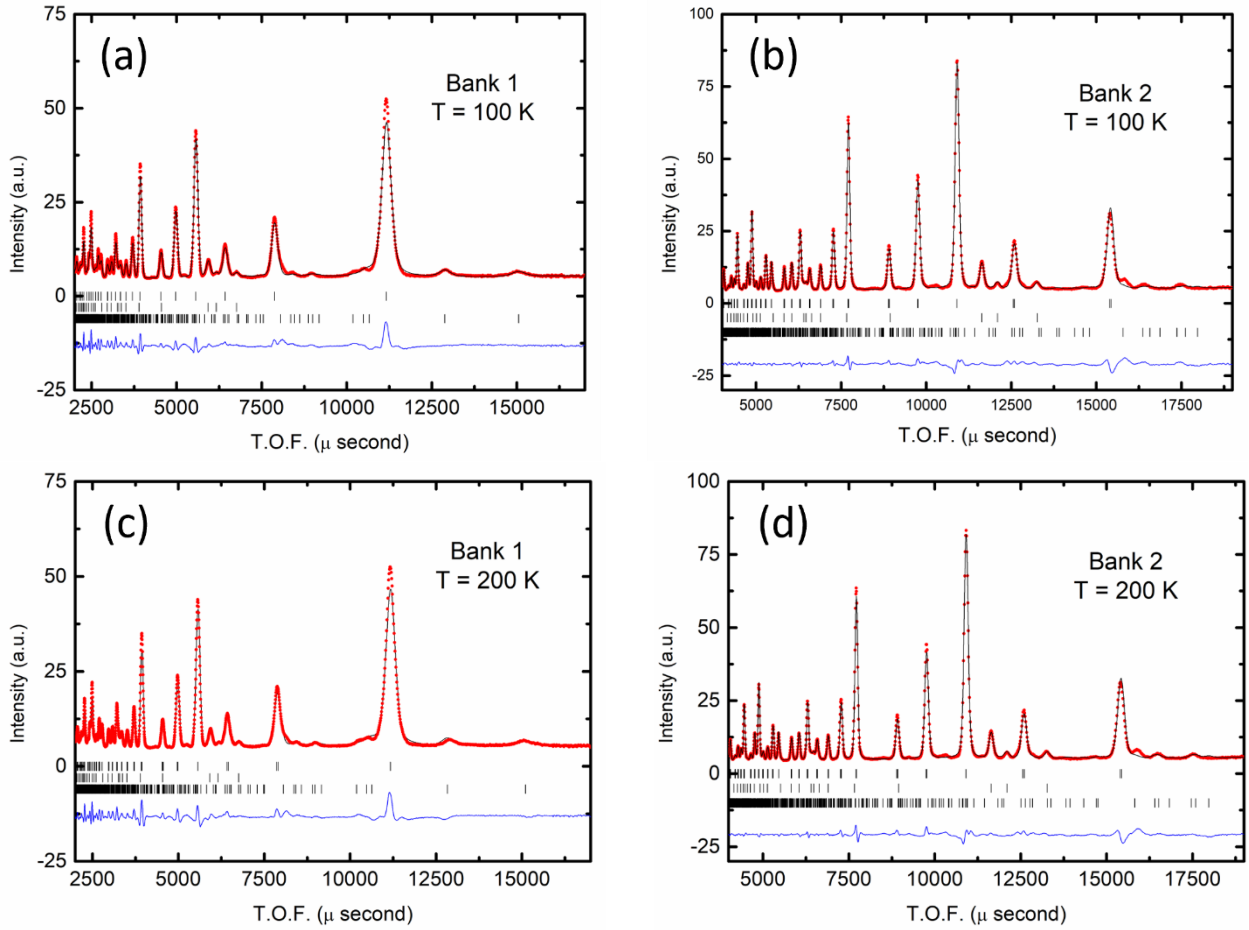

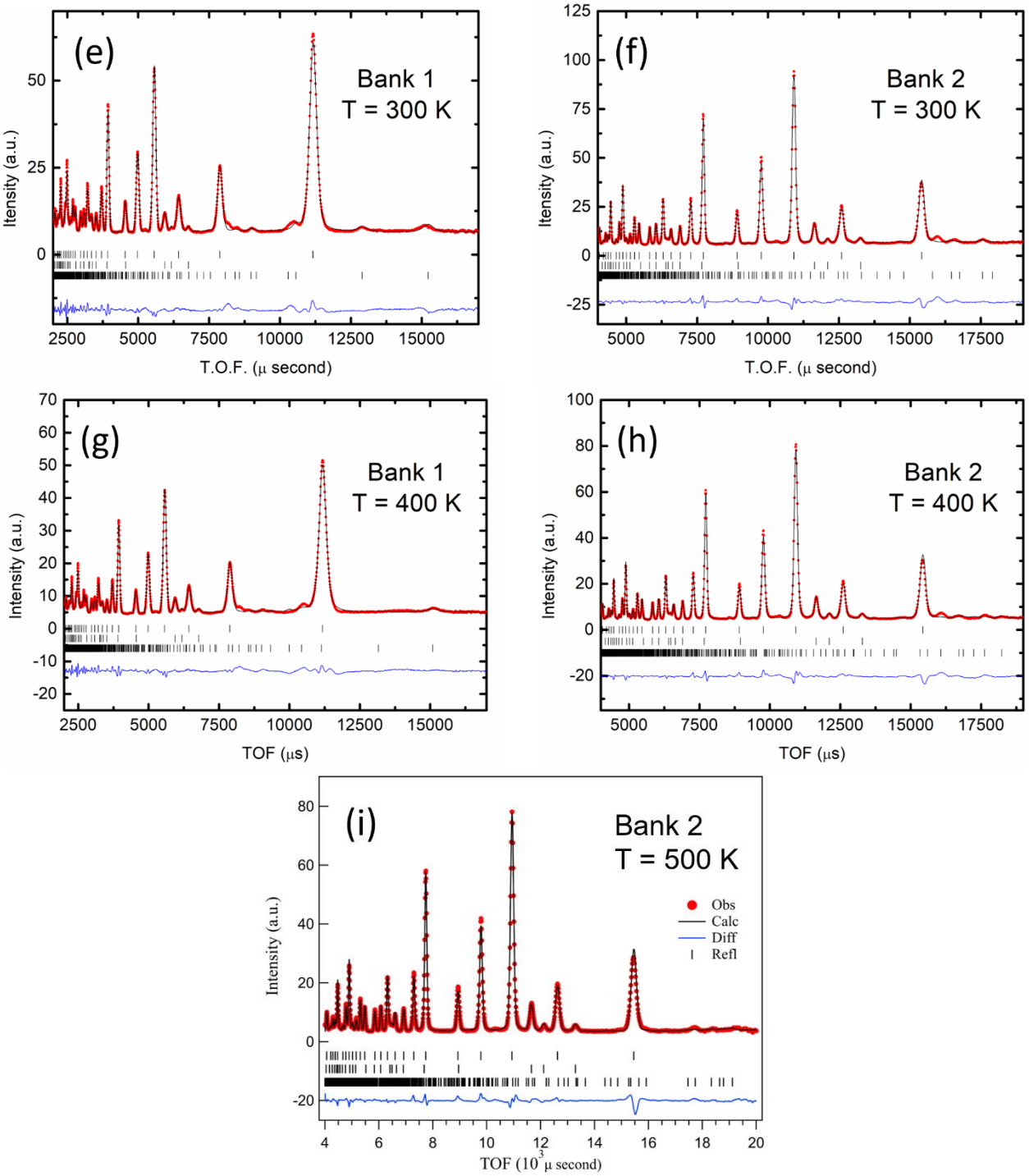

Fig. S10 Neutron diffraction patterns and the fitting results of $KOsO_3$ at different temperatures (T = 100, 200, 300, 400, and 500 K).

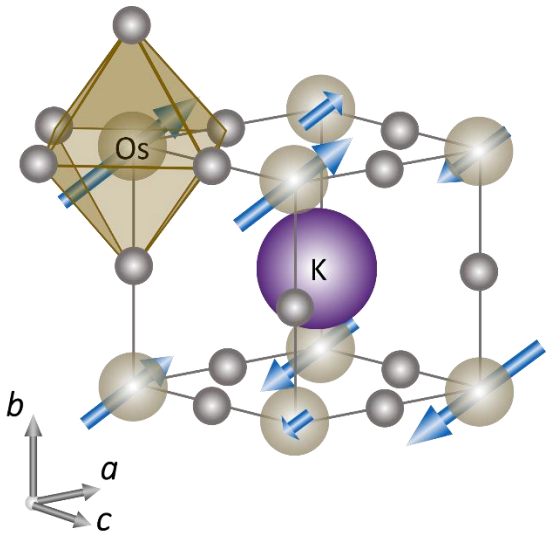

Fig. S11 The magnetic moment direction in a primary cubic cell of $KOsO_3$ deduced from neutron diffraction at 500 K

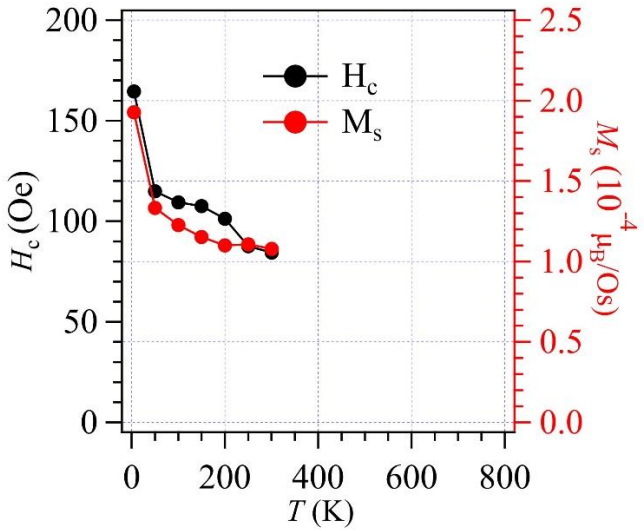

Fig. S12 Temperature dependence of the coercive force H_c and the saturation moment at 2 T for $KOsO_3$.

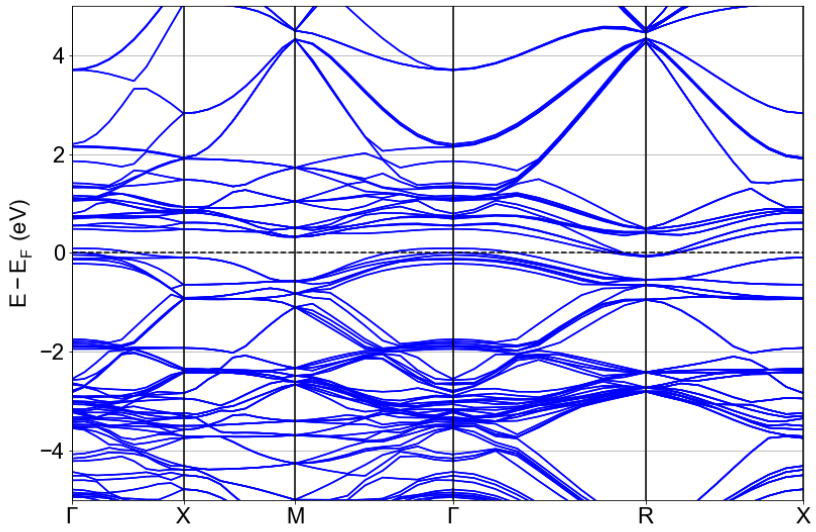

Fig. S13 The band structure of $KOsO_3$ calculated with U=1 eV +SOC.

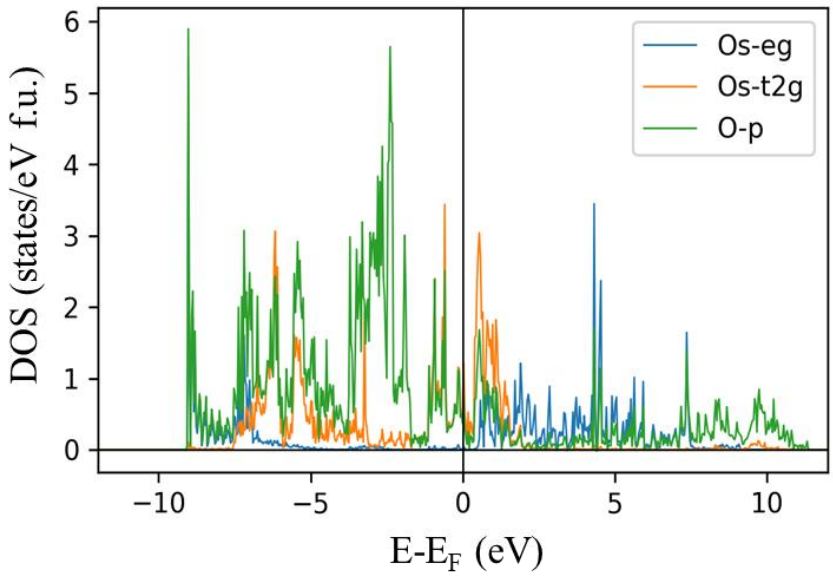

Fig. S14 The density of state derived from the band structure in Fig.S13.

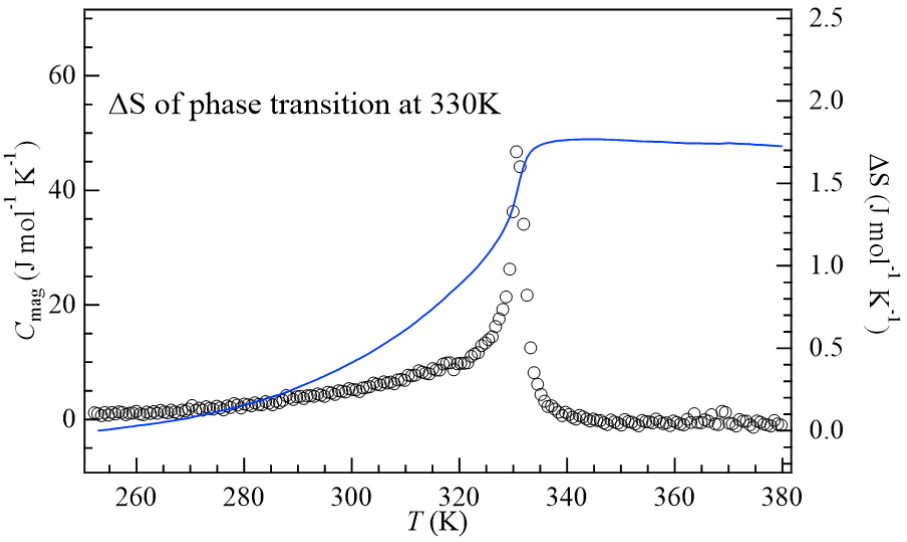

Fig.S15 The C_p after subtracting the phonon contribution versus temperature at the transition from the cubic to the tetragonal phase and the entropy change associated with the transition.

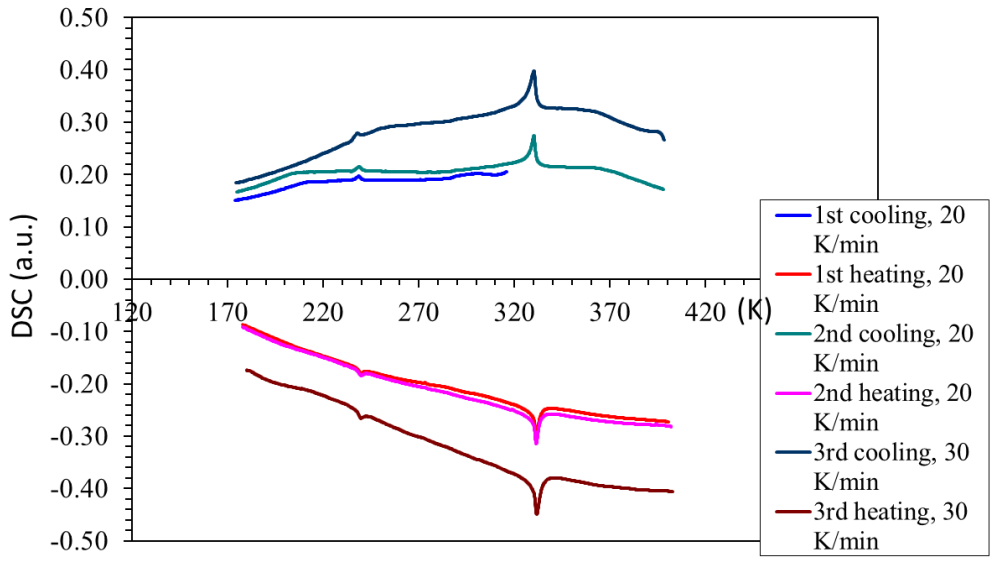

Fig.S16 Result of differential scanning calorimetry of $KOsO_3$.

Table S1. Crystallographic and structure refinement data for single crystal $KOsO_3$.

Note: Whereas the synchrotron X-ray powder diffraction pattern at room temperature in Fig.S1 shows a shoulder at a high angle peak and is refined well with the tetragonal phase model, the refinement of the single crystal diffraction gives the cubic phase.

Empirical formula	$KOsO_3$
Formula weight	277.30
Temperature	300 K
Wavelength	0.41328 Å (Synchrotron)
Crystal system	Cubic
Space group	*P m* -3 *m*
Unit cell dimensions	a = 3.89628(3) Å
Volume	59.149(1) $Å^3$
Z	1
Density (calculated)	7.785 g cm^{-3}
Absorption coefficient	13.497 mm^{-1}
F_{000}	119
Crystal size	10 × 10 × 10 μm^3
2θ for data collection	3.042– 24.699°
Index ranges	$-7 \le h \le 7$, $-7 \le k \le 7$, $-7 \le l \le 7$
Reflections collected	4033
Independent reflections	77 [R(int) = 0.0573]
Completeness to θ = 14.357°	100%
Max. and min. transmission	0.9419, 0.8640
Refinement method	Full-matrix least-squares on F^2
Data/restraints/parameters	77/0/6
Goodness-of-fit on F^2	1.106
Final R indices [I >2σ(I)]	R_1 = 0.0075, wR_2 = 0.0148
R indices (all data)	R_1 = 0.0075, wR_2 = 0.0148
Extinction coefficient	0.059(10)
Largest diff. peak and hole	0.672 and –0.828 e$Å^{-3}$

Table S2. Atomic coordinates and equivalent isotropic displacement parameters (U_{eq}, 10^{-3} $Å^2$) and anisotropic displacement parameters (U_{ij}; 10^{-3} $Å^2$) as measured by synchrotron X-ray diffraction (λ = 0.41328 Å) on a single-crystal $KOsO_3$ at 300 K.

Site	WP [a]	Occp.	x	y	z	U_{eq}
K	1*a*	1	0	0	0	6.83
Os	1*b*	1	0.5	0.5	0.5	2.59
O	3*c*	1	0	0.5	0.5	6.7
Site	U_{11}	U_{22}	U_{33}	U_{23}	U_{13}	U_{12}
K	6.83(16)	= U_{11}	= U_{11}	0	0	0
Os	2.59(6)	= U_{11}	= U_{11}	0	0	0
O	3.7 (7)	8.2(5)	= U_{22}	0	0	0

[a] Wyckoff positions; U_{eq} is defined as one third of the trace of the orthogonalized U_{ij} tensor. The anisotropic displacement factor exponent takes the form $-2\pi^2[h^2a^{*2}U_{11} + ... + 2hka^*b^*U_{12}]$.

Table S3. Bond length in $KOsO_3$ revealed by synchrotron X-ray single-crystal XRD.

Bond	Bond length (Å)	
K–O	2.75340(8) ×12	BVS (K) = 2.23
Os–O	1.94695(6) ×6	BVS (Os) = 4.87

BVS $= \sum_{i=1}^{N} v_i$, where $v_i = e^{(R_0 - l_i)/B}$, N is the coordination number, l is the bond length, B = 0.37, $R_0(K^+)$ = 2.13[22], and $R_0(Os^{5+})$ = 1.87[23].

Table S4. Atomic coordinates and equivalent isotropic displacement parameters (U_{eq}, 10^{-3} Å^2) and anisotropic displacement parameters (U_{ij}, 10^{-3} Å^2) for $KOsO_3$ at room temperature as revealed by powder synchrotron XRD (λ = 0.61928 Å) with tetragonal structural model.

Site	WP	Occp.	x	y	z	U_{eq}
K	1*a*	1	0	0	0	7.9
Os	1*d*	1	0.5	0.5	0.5	2.9
O1	1*c*	1	0.5	0.5	0	5(2)
O2	2*e*	1	0.5	0	0.5	5(1)
Site	U_{11}	U_{22}	U_{33}	U_{23}	U_{13}	U_{12}
K	8.2(4)	= U_{11}	7.3(8)	0	0	0
Os	2.9(1)	= U_{11}	3.0(3)	0	0	0

Space group: *P4/mmm* (tetragonal; no. 123); lattice constants a = 3.89488(1) Å, c = 3.89243(1) Å; cell volume = 59.0486(3) Å^3; d_{cal} = 7.799 g cm^{-3}; chemical formula sum: $KOsO_3$ (Z = 1); and the final R indices are 8.039% (R_{wp}), 6.143% (R_p), 4.034% (R_B), and 2.070% (R_F). The anisotropic displacement parameters of K and Os atoms were refined. The isotropic displacement parameters of O atoms were refined.

Table S5. Atomic coordinates and equivalent isotropic displacement parameters (U_{eq}, 10^{-3} Å^2) and anisotropic displacement parameters (U_{ij}, 10^{-3} Å^2) for $KOsO_3$ at 200 K as revealed by powder synchrotron XRD (λ = 0.61928 Å) with rhombohedral structural model.

Site	WP	Occp.	x	y	z	U_{eq}
K	3*b*	1	0	0	0.5	6.0
Os	3*a*	1	0.0	0.0	0.0	2.5
O	9*d*	1	0.5	0	0.5	4.0(3)
Site	U_{11}	U_{22}	U_{33}	U_{12}	U_{13}	U_{23}
K	5.8(3)	= U_{11}	6.4(6)	= 0.5 × U_{11}	0	0
Os	2.32(8)	= U_{11}	2.9(1)	= 0.5 × U_{11}	0	0

Space group: *R*-3*m* (rhombohedral; no. 166); lattice constants a = 5.50706(2) Å, c = 6.73481(2) Å; cell volume = 176.887(1) Å^3; d_{cal} = 7.810 g cm^{-3}; chemical formula sum: $KOsO_3$ (Z = 3); and the final R indices are 9.717% (R_{wp}), 7.686% (R_p), 3.791% (R_B), and 1.863% (R_F). The anisotropic displacement parameters of K and Os atoms were refined. The isotropic displacement parameters of O atom were refined.

Table S6. Comparison of the structural details for perovskite $KOsO_3$ formed in rhombohedral (R), tetragonal (T), and cubic (C) phases at different temperatures revealed by synchrotron X-ray powder XRD.

	C (500 K)	T (R. T.)	R (200 K)
Space group	*Pm*-3*m*	*P4/mmm*	*R*-3*m*
Lattice parameters (Å)	a = 3.89980(1)	a = 3.89488(1) c = 3.89243(1)	a = 5.50706(2) c = 6.73481(2)
Bond length K-O (Å)	2.75758(1) × 12	2.75410(1) × 4 2.75323(1) × 8	2.75353(1) × 6 2.75038(1) × 6
Bond length Os-O (Å)	1.94990(1) × 6	1.94622(1) × 2 1.94744(1) × 4	1.94608(1) × 6
Bond angle Os-O-Os (°)	180	180	180

Table S7. Irreducible representations for the little group and basis vectors for the Os atom at the site 1*a* (0,0,0) in cubic crystal structure, 1*d* (1/2, 1/2, 1/2) in tetragonal crystal structure, and 3*a* (0, 0, 0) in rhombohedral crystal structure respectively.

Irreducible representations for the little group G_{k1} = {h_1} at 500K and 400K				
propagation vector			$k_1 = (k_x, k_y, k_z)$	
	h_1		Basis function	Os (0, 0, 0)
Γ_1	1		ψ_{11} ψ_{12} ψ_{13}	(1 0 0) (0 1 0) (0 0 1)
Irreducible representations for the little group G_{k2} = {h_1, h_{27}} at 300K				
propagation vector			$k_2 = (k_x, 0, k_z)$	
	h_1	h_{27}	Basis function	Os (1/2, 0, 1/2)
Γ_1	1	1	ψ_{11}	(0 1 0)
Γ_2	1	-1	ψ_{21} ψ_{22}	(1 0 0) (0 0 1)
Irreducible representations for the little group G_{k3} = {h_1} at 200K and 100K				
propagation vector			$k_3 = (k_x, k_y, k_z)$	
	h_1		Basis function	Os (0,0,0)
Γ_1	1		ψ_{11} ψ_{12} ψ_{13}	(1 0 0) (0 1 0) (0 0 1)

Table S8. Results of the fitting of the pattern obtained in bank 1 at *T* = 500 K.

Propagation vector	k_x = 0.234(2), k_y = 0.162(3); k_z = 0.128(3)
Magnetic moment (μ_B)	m_x = 0.7(2); m_y = -0.7(1); m_z = 0.7(1); |m| = 1.19(9)
R_{Bragg} ($KOsO_3$) (%)	1.98
R_{Bragg}(Magnet.) (%)	7.28
Percentage Os (% wt.) in the hexagonal phase *P6₃/mmc*	8.7(3)

Table S9. Results of the fitting of the pattern obtained in bank 1 at *T* = 100, 200, 300, and 400 K.

Temperature (K)	400	300	200	100
Propagation vector	k_x = 0.290(2) k_y = 0.062(2) k_z = 0.202(3)	k_x = 0.286(2) k_y = 0.0 k_z = 0.181(3)	k_x = 0.105(2) k_y = 0.172(3) k_z = 0.469(4)	k_x = 0.100(2) k_y = 0.189(3) k_z = 0.448(4)
Magnetic moment (μ_B)	m_x = -1.2(1) m_y = 0 m_z = 1.32(9) |m| = 1.8(1)	m_x = 2.3(2) m_y = 0 m_z= 1.8(2) |m| = 2.9(3)	m_x = -2.1(5) m_y = -2.4(9) m_z = -1.7(6) |m| = 2.8(3)	m_x = -1.5(3) m_y = -1.08(5) m_z= -2.8(2) |m| = 3.1(1)
R_{Bragg} ($KOsO_3$) (%)	2.03	2.66	3.2	3.63
R_{Bragg}(Magnet.) (%)	16.5	16.7	14.7	13

Table S10. DFT+U, energy difference in eV per unit cell

A type	C type	G type	Ferro
0.12267	0.10289	0	0.12168

Table S11. DFT+U+SOC, energy difference in eV per unit cell

A type	G type
0.05838	0

References

10 F. Izumi, "A Rietveld-analysis program RIETAN-98 and its applications to zeolites," Mater. Sci. Forum **321**, 198-203 (2000).

11 K. Momma and F. Izumi, "VESTA 3 for three-dimensional visualization of crystal, volumetric and morphology data," J. Appl. Crystallogr. **44** (6), 1272-1276 (2011).

12 J. Neuefeind, M. Feygenson, J. Carruth, R. Hoffmann, and K. K. Chipley, "The Nanoscale Ordered MAterials Diffractometer NOMAD at the Spallation Neutron Source SNS," Nuclear Instruments and Methods in Physics Research Section B: Beam Interactions with Materials and Atoms **287**, 68-75 (2012).

13 S. Calder, K. An, R. Boehler, C. R. Dela Cruz, M. D. Frontzek, M. Guthrie, B. Haberl, A. Huq, S. A. J. Kimber, J. Liu, J. J. Molaison, J. Neuefeind, K. Page, A. M. dos Santos, K. M. Taddei, C. Tulk, and M. G. Tucker, "A suite-level review of the neutron powder diffraction instruments at Oak Ridge National Laboratory," Review of Scientific Instruments **89** (9), 092701 (2018).

14 J. Rodríguez-Carvajal, "Recent advances in magnetic structure determination by neutron powder diffraction," Physica B: Condensed Matter **192** (1), 55-69 (1993).

15 E. F. Bertaut, *Magnetism*. (New York: Academic Press., 1963).

16 G. Kresse and J. Furthmüller, "Efficient iterative schemes for ab initio total-energy calculations using a plane-wave basis set," Physical Review B **54** (16), 11169-11186 (1996).

17 G. Kresse and D. Joubert, "From ultrasoft pseudopotentials to the projector augmented-wave method," Physical Review B **59** (3), 1758-1775 (1999).
18 G. Kresse and J. Hafner, "Ab initio molecular dynamics for liquid metals," Physical Review B **47** (1), 558-561 (1993).
19 G. Kresse and J. Hafner, "Ab initio molecular-dynamics simulation of the liquid-metal--amorphous-semiconductor transition in germanium," Physical Review B **49** (20), 14251-14269 (1994).
20 U. Herath, P. Tavadze, X. He, E. Bousquet, S. Singh, F. Muñoz, and A. H. Romero, "PyProcar: A Python library for electronic structure pre/post-processing," Computer Physics Communications **251**, 107080 (2020).
21 A. Kokalj, "Computer graphics and graphical user interfaces as tools in simulations of matter at the atomic scale," Computational Materials Science **28** (2), 155-168 (2003).
22 N. E. Brese and M. O'Keeffe, "Bond-valence parameters for solids," Acta Crystallographica Section B **47** (2), 192-197 (1991).
23 J.-I. Yamaura, S. Yonezawa, Y. Muraoka, and Z. Hiroi, "Crystal structure of the pyrochlore oxide superconductor KOs_2O_6," Journal of Solid State Chemistry **179** (1), 336-340 (2006).